Robotic Double Patch Clamp Based on Interactive Mechanical Modeling for Functional Connectivity Measurement Between Neurons

Biting Ma, Jinyu Qiu, Yiwen Liu, Ruimin Li, Shaojie Fu, Yuzhu Liu, Hao Chen, Mingzhu Sun, *Member, IEEE*, Xin Zhao, *Member, IEEE* and Qili Zhao*, *Member, IEEE*

***Abstract*—Double patch clamp technique, using two micropipette electrodes to patch and measure electrophysiological signals of two neurons, is essential for investigating the functional connections between neurons in brain. However, the interactive mechanical disturbances from the dual-micropipette motions inside viscoelastic brain tissue cause dynamic drifts of neurons, making double patching low efficiency and challenging. In this paper, an interactive mechanical modeling of two micropipettes approaching two cells in elastic environment was established to estimate the dynamic drift of the cells. Based on that, a synchronous descent strategy, an appropriate relative position of two cells, and an online trajectory plan of two micropipettes were determined to improve double patch clamp efficiency. Finally, a robotic double patch clamp operation process was established for functional connectivity measurement between neurons in brain slice. The effectiveness of the proposed work is validated through both finite element modeling and experiments. The double patch clamp experiments on neurons in visual cortex demonstrate that our method achieves a 40% improvement in success rate and a 38% improvement in speed in comparison to the traditional manual method. With the above advantages, diverse functional connectivity activities between neurons were found using our system, paving a solid ground for further research.**

***Note to Practitioners*—The double patch clamp technique is a critical tool for studying the functional connectivity between neurons. However, its practical applications remain limited due to the difficulty of controlling the approach of two micropipettes to the cells, as cell drift induced by interactive mechanical disturbances often results in low success rates and a time-consuming process. This paper models the interactive mechanical disturbances between micropipettes and cells, and applies a synchronous descent strategy, an appropriate relative position of two cells, and an online trajectory plan of two micropipettes to reduce drift of cells. Through finite element modeling and experimental validation, the proposed method increases both the speed and success rate of double patch clamp experiments, and the experimental results show that the proposed method reduces dynamic drift by approximately 20%. For practitioners in neuroscience and biomedical engineering, this system provides a practical solution to reliably obtain dual-neuron recordings, enabling more efficient investigations of functional connectivity between two neurons in brain tissues. Future efforts will aim to extend the applicability of its motion control to more complex in vivo settings, where coordinated control of multiple micropipettes is required.**

***Index Terms*—Double patch, functional connectivity, microoperation, robotic patch clamp, robotic cell manipulation.**

I. Introduction

THE functional connectivity net among neurons is the basis of normal functions of neuron systems such as perception, cognition and memory formation [1], [2]. Many neuron system diseases, such as Alzheimer's disease and frontotemporal dementia [3], [4] have been proved to be related with abnormal functional connectivity among neurons. The functional connectivity measurement may provide a solution for pathological and pathogenic mechanisms research of the above neuron system diseases, and further, finding their potential treatment methods.

Since invented by Erwin Neher and Bert Sakmann in 1976 [5], patch clamp technique has become the "golden standard" for electrophysiological research of neurons due to its quantitative electrical stimulation and picoampere-level measurement accuracy with ms-level sampling intervals [6]. Specially, double patch clamp technique, using one micropipette to electrically stimulate one neuron and the other electrode to record the responding electrical signals of another neuron, is a key technology for measurement on functional connectivity between two neurons.

Taking the double patch clamp operation in brain slice as an example, the two micropipette electrodes need to pass through the brain tissue environment to approach and contact the two target neuron, aspirate part of cell membrane into micropipette opening to form a giga Ω-scale seal (gigaseal) and then break the aspirated cell membrane (break-in) to for recording the whole-cell signals. The above operation process is schematically shown in Fig. 1. To operate the two target neurons in brain slice, the operator has to move two micropipettes step by step toward to the two target cells one by one according to the visual feedback in brain slice in manual operation. As the brain tissue environment is viscoelastic, when one micropipette moves inside to approach its target cell, the generated environmental deformation not only causes the drift of its target cell, but also lead to the drift of the target cell of the other micropipette electrode, and vice versa. In summary, the above interactive mechanical disturbances resulting from motions of two micropipette electrodes lead to dynamic drifts of two target cells during double patch clamp operation. Addressing the above problem, the operator

This work was supported in part by the National Natural Science Foundation of China (62273186), Guangdong Basic and Applied Basic Research Foundation (2024A1515011171) and the Beijing Advanced Innovation Center for Intelligent Robots and Systems under Grant 2019lRS05.

Biting Ma, Jinyu Qiu, Yiwen Liu, Ruimin Li, Shaojie Fu, Yuzhu Liu, Hao Chen Mingzhu Sun, Xin Zhao and Qili Zhao are with the Institute of Robotics and Automatic Information System (IRAlS), the Tianjin Key Laboratory of Intelligent Robotic (tjKLlR), Nankai University, Tianjin 300350, China, the Engineering Research Center of Trusted Behavior Intelligence, Ministry of Education, Nankai University, Tianjin 300350, China, the Institute of Intelligence Technology and Robotic Systems, Shenzhen Research Institute of Nankai University, Shenzhen,518083, China, and also with the National Key Laboratory of Intelligent Tracking and Forecasting for Infectious Diseases, Nankai University, Tianjin 300350, China. Qili Zhao is also with the Beijing Advanced Innovation Center for Intelligent Robots and Systems, Beijing Institute of Technology, China. (correspondence e-mail: zhaoqili@nankai.edu.cn)

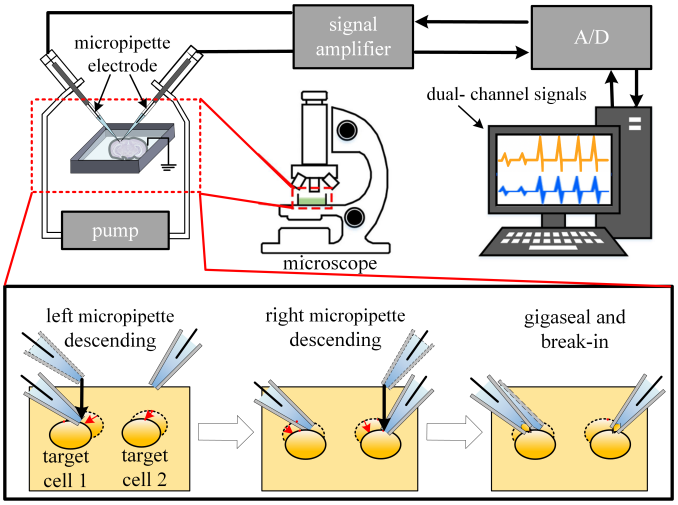

Fig. 1. The schematic of the double patch clamp on neurons in brain slices.

has to carefully and repeatedly move the two micropipettes back and forth to approach, contact and then patch the two target cells by trial and error, making the manual double patch clamp a time-consuming and labor-intensive process with low success rate. The high skill requisite and low efficiency of the manual double patch clamp significantly limit its application in brain science and neurons science. A new double patch clamp operation method is desired to improve the operation efficiency and promote its application.

In recent years, robotic patch clamp research has made substantial progress. For example, the plane patch clamp systems are the first type of commercialized automated patch clamp systems. These systems usually are equipped with a microchip with an array of microholes connecting to a pump to patch and measure multiple cells at one time [7]. However, the hole-in-plane structure makes these systems only applicable for suspended cells, which usually has no functional connectivity among them. The blind patch clamp systems are equipped with single [8] or multiple micropipette electrodes [9] to contact target cells and finish gigaseal and break-in according to measured impedance without visual feedback. These blind patch clamp systems can stimulate and measure single or multiple neurons in brain slices or even neurons in vivo. However, as lack of microscopic view guidance, the patch clamp operation success rate is usually lower in comparison to the traditional systems with microscopic view feedback. As an improvement, differential interference contrast (DIC) imaging [10] and two-photon microscopy imaging [11] depicting label-free neurons in brain slices and the fluorescent dye-labeled neurons in alive animal brains, respectively, have been utilized to guide robotic patch clamp on these cell types. However, the equipped optical path devices to view the cells significantly reduce the working space of the micropipette electrode. Therefore, most of these systems can only mount one micropipette electrode to opereate single neurons in brain slice or in vivo. Only a few systems have equipped more than one micropipette to operate single or multiple neurons and measure the functional connectivity among neurons in brain slices or in vivo according to the literature [9], [12]–[14].

The representative multiple patch clamp systems for neurons in brain slice and in vivo with view feedback are reviewed as follows. Hao et al. [15] reported a manually operated dual-arm patch clamp technique for recording mechanosensitive currents of a single cultured cell. Lewis et al. [16] applied stretch or poke stimulation and electrophysiological recording simultaneously on single cell to achieve quantitative functional characterization of mechanically activated ion channels. In our previous work, a robotic fast dual-arm patch clamp system [17], [18] was proposed to patch and record only one neuron with a micropipette electrode, and meanwhile, mechanically stimulate itself or its adjacent neuron with the other micropipette. Through kinematic modeling and three-stage motion control of two micropipette based on it, the two micropipettes can arrive at target in shorter time without collision incidences. However, as lack of interactive mechanical modeling inside brain slice, we have found that the gigaseal between one micropipette and its target cell can be easily disrupted by the mechanical disturbances resulting from further movement of the other micropipette inside brain slice environment, significantly reducing the double whole-cell patch clamp success rate for two cells. Gonzalez et al. [14] developed a robotic quad patch clamp system to approach multiple neurons in brain slices according to their initial positions without consideration of the dynamic drifts of neurons resulting from interative mechanical disturbances during four micropiepttes to approach their target cells. The success rate of achieving at least two patches simultaneously was only 42%, significantly lower than single patch success rate. Jouhanneau et al. [12] implemented a quad patch clamp system guided by two-photon microscopy for neurons in vivo. The four micropipettes are placed on the same side and descended sequentially, leading to interactive mechanical disturbances. To overcome the generated dynamic drifts of four target cells, the operator manually adjust the movement of the micropipettes back and forth, making the whole patch clamp operation time last for tens of minutes.

According to the above analysis, the interactive mechanical modeling when two micropipettes moving inside brain tissue environment is key to design appropriate trajectories of each micropipette electrode to reach its target. Wang et al. [19] developed a interactive mechanical model during the insertion of a needle into soft tissue. However, the needle is centimeter-scale in size and flexible, which is different from the micrometer-scale rigid micropipette tips used in dual-arm patch-clamp experiments, making the model unsuitable for our study. Therefore, In our previous research [20], [21], the dynamic drift of target caused by the movement of a single micropipette within intracellular space was modeled to design an appropropriate trajectory of micropieptte to reach its target. Our previous work may provide references for dynamic drifts modeling of cells as both the intracellular space and brain tissue environment are viscoelastic environment, However, different from using single micropipette to reach single target in our previous research without interactive mechanical disturbances, double patch clamp needs to control two micropipetes to reach two cells respectively with much more

complicated interactive mechanical disturbances to two cells. The interactive disturbances to two cells can be influenced by multiple factors such as the approaching strategy of the two micropipettes (one-after-another or synchronous moving) and the relative position between the two target cells. In summary, to enhance the operational efficiency of the double patch clamp technique and promote its application in functional connectivity research, it is essential to study the interactive mechanical disturbances caused by the movement of two micropipettes within brain tissue.

In this paper, an interactive mechanical modeling of two micropipette electrodes approaching two target cells in elastic environment was established to estimate the dynamic drift of two target cells in double patch clamp. Based on the above model, two target cells with appropriate relative position, a synchronous descent strategy and an online trajectory plan of two micropipettes were determined to reduce the dynamic drift of two cells for improving double patch clamp efficiency. The effectiveness of the above work was validated through both FEM modeling and experiments, and the experimental results showed that the proposed method reduced dynamic drift by approximately 20%. Finally, a robotic double patch clamp operation process was established based on above work for functional connectivity measurement between neurons in brain slice. The double patch clamp experiments on neurons in visual cortex demonstrate that our robotic double patch clamp system achieves a 40% improvement in success rate and a 38% improvement in operation speed in comparison to the traditional manual double patch method. With the above advantages, diverse functional connectivity activities including action potential transmission and excitatory regulation between neurons in visual cortex were found using our system. The above finds prove the effectiveness of the proposed system which paves a solid ground for further functional connectivity research in alive animal brain.

II. System Setup

The robotic double patch clamp system is developed based on our previous work [18], [22], as shown in Fig. 2. A standard upright microscope (Eclipse FN1, Nikon) with a 2 cm $\times$ 2 cm travel movement range in the *X-Y* plane with a repeatability of ± 0.1 μm is used to provide microscopic view feedback for patch clamp operation. The system utilizes two robotic arms to control the movement of two micropipettes. The left micromanipulator (MP-285/R, Sutter) with a travel range of 2 cm $\times$ 2 cm $\times$ 2 cm and the right micromanipulator (PatchStar, Scientifca) with a travel range of 2.5 cm $\times$ 2.5 cm $\times$ 2.5 cm and both having a maximum speed of 1 mm/s and repeatability of ± 0.1 μm are utilized to hold micropipette electrode with a tilt angle of 35°. The micropipettes are made of glass tubes (BF150-86-10, Sutter) pulling by a micropuller (P97, Sutter) and are injected with 20 uL of intracellular solution (mmol/L: K-gluconate 140, KCl 10, HEPES 10, EGTA 0.1, MgATP 0.05, Na_2GTP 0.05, and $MgCl_2$ 2, pH = 7.3) to simulate the intracellular environment of neurons. An in-house-developed pump box [22] provides pressures inside the micropipette ranging from -5 psi to 15 psi with a pressure accuracy of

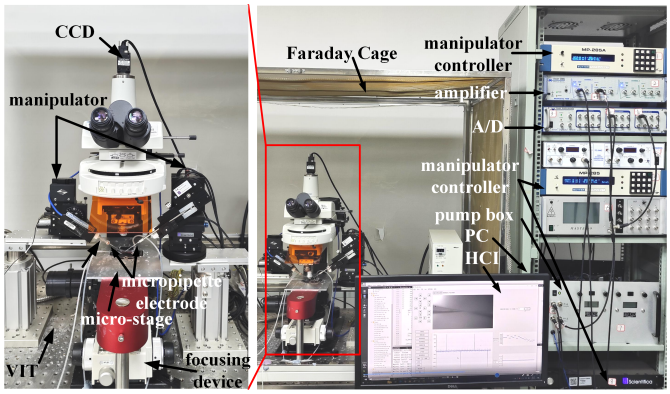

Fig. 2. Robotic double patch clamp system.

$\pm 0.1\%$ full-scale maximum pressure. A charge-coupled device (CCD) camera (lR-2000, DAGE-MTI) is mounted on the microscope to capture microscopic images at a speed of 60 fps. The entire system is mounted on a vibration isolation table (VIT) and covered with a Faraday Cage to isolate external electrical disturbances. The dual-channel electrical signals detected by micropipette electrodes are amplified by an amplifier (MultiClamp 700B, Molecular Devices), converted into digital signals (Digidata 1550B1, Molecular Devices), and then transmitted to the personal computer (PC). A human-computer interface (HCI) is developed in the PC, which is responsible for tasks such as visual feedback, the motion control of the microscope and manipulators, suction pressure control and electrical signal recording. The detailed description of HCI and preparations of brain slices can be found in Section I and Section II of the supplementary file "Supplementary file.docx".

III. Key Methods

In this section, key methods for robotic double patch clamp operation are introduced in detail. First, an interactive mechanical modeling of two micropipettes in elastic environments is established to estimate the cell drift. Subsequently, an approaching strategy of the two micropipettes and dual-target cells selection strategy were determined based on the interactive mechanical modeling. Then, motion trajectory of two micropipettes was designed to approach target cells. Based on the above work, the robotic double patch clamp operation procedure was established to improve the operation efficiency of double patch clamp in brain tissue environment.

A. Interactive Mechanical Modeling of Two Micropipettes Moving in Elastic Environments for Dynamic Cell Drift Estimation

To analyze the dynamic drifts of cells caused by the movement of two micropipette electrodes within the brain tissue, an interactive mechanical modeling is established. Initially, the tip center of each micropipette is positioned at the surface of the brain slice, directly above the center of target cell. A coordinate system *O-XYZ* is defined with the origin at the tip center of the initial position of left micropipette (LM) , the

brain slice surface as the *XY*-plane, and the depth direction as the *Z*-axis, as illustrated in Fig. 3(a). To simplify the analysis, the positions of LM and right micropipettes (RM) are defined as $P_l(x_l, y_l, z_l)$ and $P_r(x_r, y_r, z_r)$, respectively, and cell position is defined as its center position.

Subsequently, the mechanical response of the brain environments during micropipette descenting to approach target cell is analyzed. When the micropipette moves a distance d_l along the *Z*-axis, it exerts a compressive force F_1 perpendicular to the contact surface on the underlying tissue, as shown in Fig. 3(b). Given that the angle between the micropipette and the tissue plane is θ, F_1 can be decomposed into a component along the *X*-axis, F_{1X}, and a component along the *Z*-axis, F_{1Z}, according to

$$\begin{aligned} F_{1X} &= F_1 \sin\theta, \\ F_{1Z} &= F_1 \cos\theta. \end{aligned} \tag{1}$$

In addition, according to the Poisson effect, the viscoelastic brain tissue subjected to a compressive force along the *Z*-axis generates a tensile force in the *XY*-plane, as illustrated in Fig. 3(c).

Based on the above mechanical analysis, the plane L_c where the target cell is located is further analyzed. Since F_1 is generated by the displacement d_l of the micropipette, it is assumed to be proportional to d_l when d_l is small. Moreover, considering that cells farther from the micropipette experience smaller forces, F_1 is assumed to be inversely proportional to the space distance between the micropipette and cell. Therefore, the drift $d_{1X}(i, P_l)$ and $d_{1Z}(i, P_l)$ in *X*-axis and *Z*-axis of cell *i* on the L_c plane caused by F_1 can be expressed as

$$d_{1X}(i, P_l) = -\frac{k_1 d_l}{D(i, P_l; X, Y, Z)} \tag{2}$$

$$d_{1Z}(i, P_l) = \frac{k_2 d_l}{D(i, P_l; X, Y, Z)} \tag{3}$$

respectively, where k_1 and k_2 are constants related to the mechanical properties of the tissue, and $D(i, P_l; X, Y, Z)$ denotes the distance between cell *i* and the LM P_l. For F_2, experimental observations indicate that the tensile displacement in the *XY* plane is positively correlated with the distance from the micropipette within the local microscopic field. For short distances, this relationship can be approximated as linear. Therefore, the drift $d_{2X}(i, P_l)$ and $d_{2Y}(i, P_l)$ in *X*-axis and *Y*-axis of cell *i* on the L_c plane caused by F_2 can be expressed as

$$d_{2X}(i, P_l) = \frac{k_3 d_l (x_i - x_l)}{D(i, P_l; Z)} \tag{4}$$

$$d_{2Y}(i, P_l) = \frac{k_4 d_l (y_i - y_l)}{D(i, P_l; Z)} \tag{5}$$

respectively, where k_3 and k_4 are constants related to the mechanical properties of the tissue, and $D(i, P_l; Z)$ denotes the distance between cell *i* and the LM P_l along *Z*-axis direction. In the viscoelastic brain tissue, the displacement in the *XY*-plane caused by the Poisson effect is smaller than the direct compressive displacement [23]; thus, $d_{1X}(i, P_l)$ is greater than $d_{2X}(i, P_l)$. Combining (2)–(5), when the LM moves a distance d_l along the *Z*-axis, the displacements of the cell *i* in the *X*-, *Y*-, and *Z*-axis are respectively given by

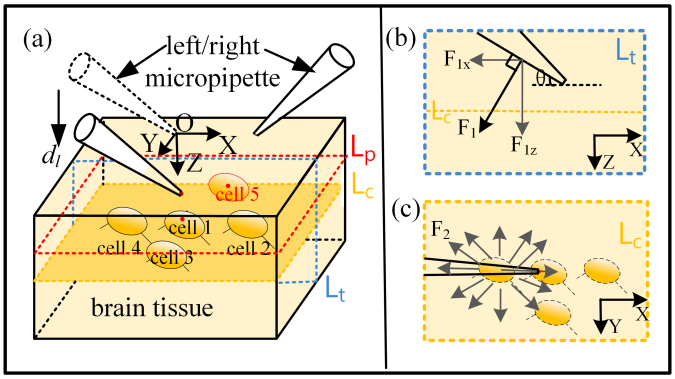

Fig. 3. Schematic diagrams of mechanical interaction between micropipettes and cells in viscoelastic brain tissue. (a) Schematic diagram of micropipette descent. (b) Schematic diagram of F_1 analysis. (c) Schematic diagram of F_2 analysis.

$$d_X(i, P_l) = -\frac{k_1 d_l}{D(i, P_l; X, Y, Z)} + \frac{k_3 d_l (x_i - x_l)}{D(i, P_l; Z)} \tag{6}$$

$$d_Y(i, P_l) = \frac{k_4 d_l (y_i - y_l)}{D(i, P_l; Z)} \tag{7}$$

$$d_Z(i, P_l) = \frac{k_2 d_l}{D(i, P_l; X, Y, Z)}. \tag{8}$$

Similarly, when the RM moves a distance d_l along the *Z*-axis, based on the above analysis, the displacements of the cell *i* along the *X*-, *Y*-, and *Z*-axes are respectively given by

$$d_X(i, P_r) = \frac{k_1 d_l}{D(i, P_r; X, Y, Z)} + \frac{k_3 d_l (x_i - x_r)}{D(i, P_r; Z)} \tag{9}$$

$$d_Y(i, P_r) = \frac{k_4 d_l (y_i - y_r)}{D(i, P_r; Z)} \tag{10}$$

$$d_Z(i, P_r) = \frac{k_2 d_l}{D(i, P_r; X, Y, Z)}. \tag{11}$$

Interactive mechanical modeling of the dynamic drifts of two target cells with two micropipettes moving in brain environments are estimated based on (6)-(11) and subsequently applied to dual-cell selection and trajectory design of the two micropipettes.

B. Approaching Strategy Determination and Dual-target cells Selection Based on the Interactive Mechanical Modeling

As mentioned in Introduction, the approaching strategy of the micropipettes to reach two target cells (one-after-another or synchronized moving), as well as the relative position of the two target cells can affect interactive mechanical disturbances to two cells with two micropiepttes moving inside brain tissue environment. In this section, appropriate approaching strategy and relative positions of the two cells are determined based on the established interactive mechanical modeling to reduce the dynamic drifts of the two cells for improving the operation efficiency of the double patch clamp in brain tissue environment.

1) Approaching strategy determination based on the interactive mechanical modeling: Based on (8) and (11), movement of the one micropipette along the *Z*-axis induces the dynamic drift of cells in the same direction. Therefore, if a micropipette moves down to approach and patch the target cell first in *Z*-axis direction, the subsequent descent of the other micropipette to its target cells may displace the first cell along the *Z*-axis, enlarging the distance or disrupting the established patch between the first micropipette and its target cell. In that case, back and forth moving the two micropipettes may be needed to finally approach and patch both two cells, cost long operation time of double patch clamp. In comparison, synchronous descent of the two micropipettes until they approach the two cells both in *Z*-axis direction can prevent repeated adjustment of position of two micropipettes back and forth, which saves operation time. Besides, based on (6) and (9), synchronous descents of the LM and RM exerts opposing displacements on the same cell along the *X*-axis, effectively offsetting each other and thereby reducing cell drift in *X*-axis.

In summary, a synchronous descent strategy is determined based on above analysis.

2) Appropriate relative position determination for two target cells based on interactive mechanical modeling: Subsequently, appropriate relative position of two target cells were determined to reduce the dynamic drifts of two cells with two micropipettes synchronous approaching them. In this way, the operation efficiency of double patch clamp can be further improved through choosing two cells with the determined appropriate positions in the field of view as the dual target cells.

First, the appropriate relative positions of two target cells in the same horizontal plane is determined based on the developed interactive mechanical model. As shown in Fig. 3(a), cell 1 at the $(0, 0, z_c)$ is fixed as the target cell for the LM, while cells positioned at the same distance r from cell 1 in same horizontal plane but at different orientations are considered as candidate target cells for the RM. The candidate cells including cell 2 at $(r, 0, z_c)$, cell 3 at $(0, r, z_c)$ and cell 4 at $(-r, 0, z_c)$. Assuming the two micropipettes are located at positions just above the two target cells at first, then the two micropipettes moves downward by d_l to approach the two cells. The drifts of the two target cells caused by the motion of two micropipettes are calculated to get the combined drift of one target cell. When cell 2, cell 3 or cell 4 is selected as target cell of the right cell, due to the geometrical symmetry of the dual-micropipette configuration relative to the target cells, the drifts of the two cells can be approximated as equivalent. Thus, only the combined drift of cell 1 is calculated based on the interactive mechanical model in above three cases.

Since the micropipettes are parallel to the *X*-axis, the opening as well as the neighboring segment enter the brain tissue environment during the approach, the effective *X*-axis of each micropipette is assumed to be located at a distance r_1 from the opening. Therefore, the reference point of the left (x_l, y_l, z_l) is approximated as $(-r_1, 0, 0)$. First, the drift of cell 1 caused by LM is calculated using (6)–(8) as

$$d_X(cell1, P_l \rightarrow cell1) = -\frac{k_1 d_l}{\sqrt{r_1^2 + z_c^2}} + \frac{k_3 d_l r_1}{z_c} \tag{12}$$

$$d_Y(cell1, P_l \rightarrow cell1) = 0 \tag{13}$$

$$d_Z(cell1, P_l \rightarrow cell1) = \frac{k_2 d_l}{\sqrt{r_1^2 + z_c^2}}, \tag{14}$$

where $d_X(cell1, P_l \rightarrow cell1)$, $d_Y(cell1, P_l \rightarrow cell1)$ and $d_Z(cell1, P_l \rightarrow cell1)$ represent the drift components of cell 1 caused by LM in the *X*, *Y*, and *Z* directions, respectively.

When cell 2 is selected as the target cell for RM, the reference point (x_r, y_r, z_r) of RM is ($r + r_1$, 0, 0). Based on (9)-(11), the drift of cell 1 caused by RM moving downward to cell 2 can be calculated as

$$d_X(cell1, P_r \rightarrow cell2) = \frac{k_1 d_l}{\sqrt{(r + r_1)^2 + z_c^2}} - \frac{k_3 d_l (r + r_1)}{z_c} \tag{15}$$

$$d_Y(cell1, P_r \rightarrow cell2) = 0 \tag{16}$$

$$d_Z(cell1, P_r \rightarrow cell2) = \frac{k_2 d_l}{\sqrt{(r + r_1)^2 + z_c^2}}, \tag{17}$$

where $d_X(cell1, P_r \rightarrow cell2)$, $d_Y(cell1, P_r \rightarrow cell2)$ and $d_Z(cell1, P_r \rightarrow cell2)$ represent the drift components of cell 1 caused by RM in the *X*, *Y*, and *Z* directions, respectively. According to (12)-(17), the drift components of cell 1 caused by two micropipettes in the *X*, *Y*, and *Z* directions are

$$\begin{aligned} &d_X(\text{cell 1},\ P_l \rightarrow \text{cell 1},\ P_r \rightarrow \text{cell 2}) \\ &\quad = -\frac{k_1 d_l}{\sqrt{r_1^2 + z_c^2}} + \frac{k_1 d_l}{\sqrt{(r + r_1)^2 + z_c^2}} - \frac{k_3 d_l r}{z_c} \end{aligned} \tag{18}$$

$$d_Y(\text{cell 1},\ P_l \rightarrow \text{cell 1},\ P_r \rightarrow \text{cell 2}) = 0 \tag{19}$$

$$\begin{aligned} &d_Z(\text{cell 1},\ P_l \rightarrow \text{cell 1},\ P_r \rightarrow \text{cell 2}) \\ &\quad = \frac{k_2 d_l}{\sqrt{r_1^2 + z_c^2}} + \frac{k_2 d_l}{\sqrt{(r + r_1)^2 + z_c^2}} \end{aligned} \tag{20}$$

respectively, and are hereinafter abbreviated as d_X, d_Y, and d_Z.The total drift of cell 1 $d(cell1, P_l \rightarrow cell1, P_r \rightarrow cell2)$ can be obtained by calculating the square root of the sum of the drift components' squares.

When cell 3 is selected as the target cell of RM, the reference point (x_r, y_r, z_r) of RM is $(r_1, r, 0)$. Based on (9)-(11), the drift of cell 1 caused by RM moving downward to cell 3 is

$$d_X(cell1, P_r \rightarrow cell3) = \frac{k_1 d_l}{\sqrt{r^2 + r_1^2 + z_c^2}} - \frac{k_3 d_l r_1}{z_c} \tag{21}$$

$$d_Y(cell1, P_r \rightarrow cell3) = -\frac{k_4 d_l r}{z_c} \tag{22}$$

$$d_Z(cell1, P_r \rightarrow cell3) = \frac{k_2 d_l}{\sqrt{(r^2 + r_1^2 + z_c^2}}, \tag{23}$$

In this case, the drift components of cell 1 caused by RM in the *X*, *Y*, and *Z* directions (denoted as $d_X(cell1, P_l \rightarrow cell1, P_r \rightarrow cell3)$), $d_Y(cell1, P_l \rightarrow cell1, P_r \rightarrow cell3)$) and $d_Z(cell1, P_l \rightarrow cell1, P_r \rightarrow cell3)$), respectively) as well as the total drift $d(cell1, P_l \rightarrow cell1, P_r \rightarrow cell3)$, can

be obtained using the same calculation method as described above.

When cell 4 is selected as the target cell of RM, the reference point (x_r, y_r, z_r) of RM is $(r_1 - r, 0, 0)$. Based on (9)-(11), the drift of cell 1 caused by RM moving downward to cell 4 is

$$d_X(cell1, P_r \rightarrow cell4) = \frac{k_1 d_l}{\sqrt{(r_1 - r)^2 + z_c^2}} - \frac{k_3 d_l (r_1 - r)}{z_c} \tag{24}$$

$$d_Y(cell1, P_r \rightarrow cell4) = 0 \tag{25}$$

$$d_Z(cell1, P_r \rightarrow cell4) = \frac{k_2 d_l}{\sqrt{((r_1 - r)^2 + z_c^2}}, \tag{26}$$

In this case, the drift components of cell 1 caused by RM in the *X*, *Y*, and *Z* directions (denoted as $d_X(cell1, P_l \rightarrow cell4, P_r \rightarrow cell4)$), $d_Y(cell1, P_l \rightarrow cell1, P_r \rightarrow cell4)$) and $d_Z(cell1, P_l \rightarrow cell1, P_r \rightarrow cell4)$), respectively) as well as the total drift $d(cell1, P_l \rightarrow cell1, P_r \rightarrow cell4)$, can be obtained using the same calculation method as described above.

Figure 4(a) intuitively illustrates the dynamic drift direction and magnitude of cell 1 when cell 2-cell 4 are selected as the target cells of RM, respectively. The black arrows stand for the drift of cell 1 caused by LM along different directions, which remains constant according to (12)-(14). It can be found that the movement of the LM primarily induces drift of cell 1 in the *XZ* plane. When cell 3 is selected, the movement of the RM additionally induces drift of cell 1 in the *Y*-direction $d_Y(cell1, P_r \rightarrow cell3)$ based on (21), making the overall drift more complex. Based on (12)-(14) and (24)-(26), when cell 4 is selected, it can be found that $d_Z(cell1, P_r \rightarrow cell4)$¿$d_Z(cell1, P_l \rightarrow cell1)$ and $d_X(cell1, P_r \rightarrow cell4)$¿$d_X(cell1, P_l \rightarrow cell1)$, which means the dynamic drift of cell 1 caused by RM moving toward to cell 4 is larger than that caused by LM moving downward to cell 1. In that causes cell 1 to move away from the LM with a larger drift along the *Z* and *X* directions, which increases difficulties for LM to reach and patch cell 1. Moreover, the staggered opposing arrangement of the two micropipettes increases the risk of collision. In comparison, when cell 2 is selected as the target cell for the RM, the *Z*-direction drift of cell 1 $d_Z(cell1, P_r \rightarrow cell2)$ is relatively small, and the *X*-direction drift $d_X(cell1, P_r \rightarrow cell2)$ can partially offset drift $d_X(cell1, P_l \rightarrow cell1)$ induced by the LM. Therefore, cell 1-cell 2 pair is prioritized as the targets for two micropipettes in experiments.

To further evaluate the influences of the relative positions of two cells in vertical direction on interactive mechanical disturbances, cell 1 and cell 5 are located at below and above the plane by $\frac{\sqrt{2}}{4}r$ respectively and with an distance r with each other and with a coordinates $(0, 0, z_c)$ and $(\frac{\sqrt{2}}{4}r, 0, z_c - \frac{\sqrt{2}}{4}r)$, respectively. When the two micropipettes descend at the same speed, the RM will reach the cell 5 first. As a result, the subsequent descend of LM may cause disturbance to cell 5, and cell 1 loses counteracting drift in the *X*-direction from the movement of RM, denoted as $d_X(cell1, P_r \rightarrow cell5)$. When the two micropipettes descend at the different speed to reach targets simultaneously, the per-second descent distance of RM is smaller than that of the LM, making a smaller counteracting drift $d_X(cell1, P_r \rightarrow cell5)$ and a larger drift of cell 1 in the *X*-direction $d_X(cell1, P_l \rightarrow cell1, P_r \rightarrow cell5)$ according to (6) and (9). Additionally, the use of different descent speeds increases the complexity of control. Therefore, selecting cell pairs at different depths is unsuitable for stable dual-micropipette contact with the dual-cell. Unless it is necessary to record neurons at different depths, laterally-symmetric cells within the same focal plane is prioritized as targets for double patch clamp operation based on the above analysis.

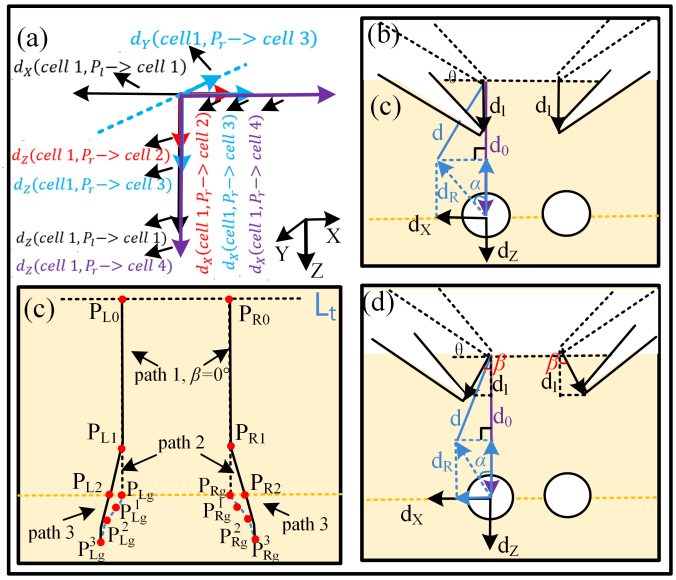

Fig. 4. Analysis of the drift of target cells and the trajectory design of micropipettes. (a) The drift direction and magnitude of cell 1 when different target cells are selected. (b) Schematic diagram of drift analysis of target cell when the micropipettes descend along *Z*-axis. (c) The trajectory design of micropipettes. (d) Schematic diagram of drift analysis of target cell when the micropipettes descend with a β angle.

C. Motion Trajectory Design for Two Micropipettes to Approach Target Cells

Based on the above analysis, the two cells in the same horizontal plane and with relative positions parallel with *X* axis direction, which corresponds to the projection direction of the two micropipettes, are preferred to be two target cells for reducing the mechanical disturbance when two micropipettes approach them. As shown in Fig. 4(c), the cell drift d_R relative to the target micropipette can be derived based on geometric relationships

$$d_R = \sqrt{(d_Z - d_l)^2 + d_X^2}. \tag{27}$$

A vertical descent by a distance d_l along the *Z*-axis of the micropipette above the cell leads to a deviation angle α

$$\alpha = \arctan \frac{d_X}{d_l - d_Z}. \tag{28}$$

As shown in Fig. 4(d), when the micropipette approaches the cell at an inclined angle β, the α is updated as

$$\alpha = \arctan \frac{d_X - d_l \tan \beta}{d_l - d_Z}. \tag{29}$$

Therefore, the α can be reduced to zero by gradually controlling the micropipette movement angle β.

During the experiment, the β is dynamically determined based on the drift of cells, and the detailed determination process of β can be found in Section IV of the supplementary file "Supplementary file.docx". According to (18) and (20), when the initial distance between the micropipette and cell is large, the cell drift is relatively small. Therefore, the trajectories of micropipettes are designed in three paths, as illustrated in Fig. 4(b). In path 1, the micropipettes descend three-quarters of the initial distance d_0 along the Z-axis to P_{L1} and P_{R1} to accelerate the approaching process. Then, the dynamic drift direction and magnitude of the cell are detected through mouse click, and the parameters β and d_l for path 2 are updated accordingly, guiding the micropipettes to P_{L2} and P_{R2}. Then, the dynamic drift direction and magnitude of the cell are detected again. In path 3, the micropipettes descend with updated angle β. When the bath resistance increases by 0.1 MΩ, it is considered that the micropipette have made initial contact with the cell. The micropipette then reduces its speed and continues to descend vertically until a close contact with the cell is established according to the significant rise of the detected resistance of micropipette electrode.

D. Robotic double patch clamp operation procedure

Based on the above work, the robotic double patch clamp operation procedure is established. Before the experiment, the workspace calculation for the dual-arm and the placement of the brain slice are implemented based on previous methods [18] to guide the two micropipette tips to arrive at the brain slice surface position above the two target cells.

The experimental procedure is shown in Fig. 5. First, the two micropipettes are focused under a 4× microscope using coarse-stage control and focused under a 40× microscope using fine-stage control methods [18], [24]. Then, the objective lens continues descending until the brain tissue is in focus, as identified by the temporal standard deviation difference using a sliding window approach [25]. Then, the objective lens descends a further 20-50 μm to focus on a deeper plane where cellular structures are better preserved, and two target cells are identified through YOLOv7 [26] and selected based on the aforementioned dual-cell selection strategy. The detailed method can be found in Section V of the supplementary file "Supplementary file.docx". If the operator is not satisfied with the result, the cell pair can be selected through mouse click. Then, the two micropipettes are moved directly above the target cells based on the precise-stage control method. Next, the two micropipettes are synchronously descended to the cell surface according to online-designed trajectories introduced in Section III(C). During this process, the drift in XY-plane are obtained by measuring the center position variation in XY-plane of cells. The drift in Z-axis are obtained by measuring the position variation in Z-axis of objective focusing target cells. Based on the detected drift, the trajectories of micropipettes are dynamically adjusted. When the bath resistance increases by 0.1 MΩ in Path 3, it is considered that the micropipette have made initial contact

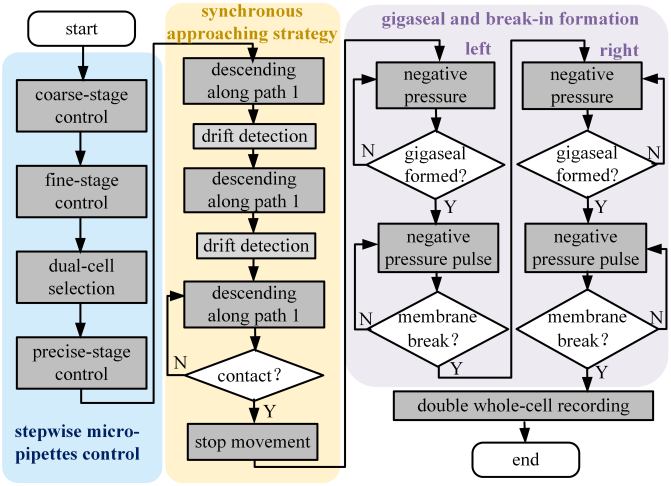

Fig. 5. Diagram of robotic double patch clamp operation procedure.

with the cell. Therefore, the β is reset to 0 and the speed is decreased to avoid piercing the cell, and a resistance-based method is used to establish close contact with the cells respectively [22]. Once the increased bath resistance reaches a threshold within the range of [0.6–0.9] MΩ, the movement is stopped. Then, a robotic whole-cell patch clamp method is used to sequentially form gigaseal between each micropipette and its target cell through exerting an aspiration pressure of -0.5 psi, and then applies a series of negative pulses with magnitudes of 5 psi to break the aspirated cell membrane [18], [20], [24], ultimately forming a double whole-cell state. The detailed operation process of above procedures are shown in the uploaded supplementary file "Robotic double patch clamp process.mp4".

After that, one micropipette electrode applies electrical stimulation (ES) to its target cell to activate it and records the electrophysiological signals. At the same time, the other micropipette electrode records the electrophysiological signals of the other target cell without stimulation. This setup allows for the simultaneous acquisition of electrophysiological signals from two neighboring cells, enabling analysis of their synaptic connectivity functions [27]. The above stimulation and recording process can be found in the uploaded suplementary file "Double whole-cell recording.mp4".

IV. Simulation And Experimental Results

In this section, finite element simulations and a series of experiments on neurons in visual cortex of mouse brain slices were conducted to validate the effectiveness of the above key methods and the proposed robotic double patch clamp system in Section III. First, finite element simulations within a brain tissue environment were conducted to validate the proposed interactive mechanical model. In brain slice experiments, micropipettes approaching to neurons were conducted to validate the interactive mechanical model and the selection strategy of dual-cells. Then, robotic double patch clamp experiments were conducted to validate the proposed strategies of dual-cell selection and trajectory design, finally demonstrating the

effectiveness of the proposed robotic double patch clamp system.

All experimental procedures involving mice were approved by the Committee for Animal Experimentation of the College of Life Sciences at Nankai University (No. 2008) and were performed in accordance with the NIH Guide for the Care and Use of Laboratory Animals (No. 8023, revised in 1996).

A. Validation Results of Interactive Mechanical Model Through Finite Element Simulation and Approaching Experiments

In finite element simulations, simulations of single-micropipette descent were performed to validate the interactive mechanical model firstly. Then, simulations of sequential and synchronous descent strategies of dual-micropipette descent were conducted respectively to demonstrate that the latter is better for reducing dynamic drifts of two target cells. Then, simulations of dual-micropipette descent synchronously to dual cells with different relative positions were conducted to validate the dual-cell selection strategy. The above simulations are presented in detail in Section III of the supplementary file "Supplementary file.docx", "Simulation 1.mp4", "Simulation 2.mp4", and "Simulation 3.mp4".

In brain slice experiments, LM approaching to neurons were conducted to validate the interactive mechanical model firstly. Then, experiments of dual-micropipette approaching to dual-cells at different orientations synchronously were conducted to further validate the selection strategy of dual-cells. The results indicate that selecting the cell 1–cell 2 pair is the optimal configuration for minimizing interactive disturbance. The detailed description can be found in Section VI of the supplementary file "Supplementary file.docx".

B. Robotic Double Patch Clamp Experimental Results

To validate the effectiveness of the proposed robotic double patch clamp operation process, the number of 60 robotic double patch clamp experiments were conducted on brain slice, involving cell pairs with different spatial orientations and different descent sequences, and each experimental condition was repeated 10 times to reduce random error. The average success rate of double whole-cell recordings and the average operation time were used to evaluate the performance of different strategies.

The results of above experiments are summarized in Table I. When the descent sequence was treated as a variable, strategy of synchronous descent consistently showed higher success rates (70% vs. 50% for cell 1–2; 50.0% vs. 40% for cell 1–3; 20% vs. 20% for cell 1–4), and shorter operation times (11.7±1.9 min vs. 12.8±1.3 min for cell 1–2; 13.3±2.5 min vs. 13.8±0.9 min for cell 1–3; 14.2±0.2 min vs. 14.4±0.6 min for cell 1–4) than sequential descent across all cell pairs. The binary logistic regression results showed that the descent strategy had no significant effect on the success rate ($p = 0.43$), and the one-way ANOVA indicated that the difference in operation time was also not statistically significant ($F(1, 23) = 1.20$, $p = 0.28$). Nevertheless, effect size analysis demonstrated that synchronous descent increased the odds of success by 1.5 times (OR = 1.51), and produced a reduction in operation time ($\eta^2 = 0.05$) compared to sequential descent. When focusing on synchronous descent, in experiments where the cell pair was treated as variable, selecting cell 1–cell 2 pair achieved the highest success rate (70% vs. 50.0% for cell 1–cell 3 pair ($p = 0.37$) and 20% for cell 1–cell 4 pair ($p = 0.033$) and the shortest operation time ($F(2, 11)=1.44$, $p = 0.28$). Effect size analysis further demonstrated that cell 1–cell 2 increased the odds of success by approximately 2.3 times (OR = 2.33) compared with the cell 1–cell 3 pair and by about 9.1 times (OR = 9.09) compared with the cell 1–cell 4 pair, while achieving the best operation speed performance ($\eta^2 = 0.21$). Therefore, the results demonstrate that the proposed strategies of dual-cell selection and trajectory design lead to lower mechanical disturbance, and our robotic system is capable of operating neurons in mouse brain slices with a success rate of 70% (n=10) at an average speed of 11.7±1.9 min/experiment (n=7). Among the 3 failed cases, one was due to excessive contact between micropipette and cell, resulting in cell rupture. This occurred because the close contact was assessed solely by change of micropipette resistance with an empirical threshold of [0.6–0.9] MΩ. However, variations in the mechanical properties of different cells lead to different trends in resistance increase. Therefore, a fixed resistance threshold may cause excessive or insufficient contact, resulting in membrane rupture or unstable attachment, respectively. The other 2 failures were caused by seal instability during break-in operation, leading to unsuccessful whole-cell mode formation. The experimental settings that contributed to seal instability included the fixed resistance threshold, a constant aspiration pressure of –0.5 psi to seal and pressure pulses of 5 psi to break the aspirated cell membrane, which may cause the aspirated membrane to loosen or even detach from the micropipette wall. Beyond these failures, no instances of micropipette clogging were observed across all 60 experiments.

TABLE I
ROBOTIC DOUBLE WHOLE-CELL PATCH CLAMP OPERATION RESULTS

cell pairs	descent sequence	average double whole-cell recording rate	average operation time (min)
cell 1–cell 2	1	0.5 (5/10)	12.8 ± 1.3
	2	0.7 (7/10)	11.7 ± 1.9
cell 1–cell 3	1	0.4 (4/10)	13.8 ± 0.9
	2	0.50 (5/10)	13.3 ± 2.5
cell 1–cell 4	1	0.2 (2/10)	14.4±0.6
	2	0.2 (2/10)	14.2 ±0.2

*For descent sequence, 1 presents sequential descent, and 2 presents synchronous descent.

We compared the performance of the proposed method with recently reported automated multi-patch clamp systems, as shown in the Table II. Previous automated systems achieved success rates ranging from 30% to 63% and required similar operation times. Automated four-arm patch clamp systems with visual feedback for in vitro (brain slices) [14] and in vivo [12] achieved success rates of 42% (5/12) and 63% (26/41), respectively, for establishing at least 2 whole-cell recordings. The in vivo blind multiple patch clamp system [9] achieved a

success rate of 30.7% (13/41) and an operation time of 10.5 ± 2.6 min/experiment (n = 13). Furthermore, the number of 10 experiments conducted manually by an operator with more-than-two-year experience in single patch clamp operation has a success rate of 50% (5/10) at an average speed of 19±5 min/experiment. These results demonstrate that our approach effectively improves the success rate of double whole-cell recordings by reducing the mechanical disturbances.

TABLE II
PERFORMANCE COMPARISON

method	success rate (whole-cell recording>1)	operation time (min)
Two-photon quadruple patch clamp in brain slices [14]	42% (5/12)	/
In vivo two-photon quadruple patch clamp [12]	63% (26/41)	/
In vivo blind quadruple patch clamp [9]	30.7% (13/41)	10.5±2.6 (n=13)
Proposed method	70% (7/10)	11.7±1.9 (n=7)

Figure 6 illustrates an experimental process of dual-micropipette and dual-cell contact based on cell 1-cell 2 pair selection and proposed trajectory design. Figure 6(a) from top to bottom shows the sequential changes in the positions of the cells and micropipettes in microscopic images, which are overlaid in an image, as shown in Fig. 6(b). It can be observed that the cells drifted primarily along the X-axis toward their respective micropipettes, and the micropipettes were adjusted accordingly. The position relationship of the cells and micropipettes along the Z-axis in this experiment is presented by the blue line in Fig. 6(c), while gray lines correspond to other trials. The data indicate that cells exhibited considerable drift along the Z-axis, which increased more rapidly as the micropipettes approached. Despite this drift, successful contact between the cells and the micropipettes was ultimately achieved, demonstrating the effectiveness of the proposed methods.

C. Functional Connectivities Measurement Results

Electrophysiological signals of double whole-cell recordings obtained from the robotic double patch clamp experiments are shown in Fig. 7. In the successful experiments, only 8% (2/25) exhibits presynaptic and postsynaptic signals, primarily because most adjacent neurons are not functionally connected. This result is consistent with previous studies, which reported that only approximately 10% of adjacent neurons exhibit synaptic connectivity [27].

The presynaptic and postsynaptic signals under different stimulation protocols are presented in Fig. 7(a)-(c). The Fig. 7(a) displays action potentials (APs) of cell 1 induced by ES, which subsequently trigger excitatory postsynaptic potentials (EPSPs) in cell 2. The Fig. 7(b) shows the ion channel currents of cell 1 caused by ES, leading to EPSCs in cell 2. The Fig. 7(c) illustrates the EPSCs generated of cell 1 and cell 2 when the membrane potential is clamped at -70 mV. Additionally, figure 7(b) compares the recorded voltage traces of dual cells with (left) and without (right) functional connectivity, when current stimulation was applied only to cell 1. In the left, APs generated in cell 1 triggered EPSPs in cell 2, indicating functional connectivity. In contrast, the right shows no such response in cell 2. These results demonstrate the existence of synaptic transmission between the two cells, consistent with previous studies on functional connectivity in cortical networks [12], [27].

Furthermore, figure 7(c) illustrates the double whole-cell recordings of a single experiment in which current stimulation were sequentially performed on cell 1 or cell 2 (from R1 to R4), and the lines in different colors represent voltage traces recorded under different stimulation intensities (from 60 pA to 200 pA). An intriguing observation emerged from this sequence: in R1, ES was applied only to cell 1, but no APs were observed. In R2, ES to cell 2 evoked APs, while no response was detected in cell 1. When ES was reapplied to cell 1 in R3 again, it elicited dense APs, markedly different from the response in R1, and the resting membrane potential of cell 1 shifted from -35 mV in R1 to a more physiological -60 mV in R3. In R4, ES to cell 2 again induced APs, and corresponding EPSPs were observed in cell 1. This dynamic process shows that cell 1 exhibited distinct electrophysiological responses under comparable stimulation conditions. However, the emergence of corresponding EPSPs in R4 and the restored excitability of cell 1 in R3 suggest that cell 2 may modulate the excitability of cell 1 either through neurotransmitter release or by altering the extracellular environment [28]. A detailed presentation of the electrophysiological signals shown in Fig. 7 can be found in Section VII of the supplementary file "Supplementary file.docx".

These results demonstrate that our robotic double patch-clamp system is capable of simultaneously recording the electrophysiological activites of two neurons within the brain environment, showing great potential for functional connectivity measurements between neurons.

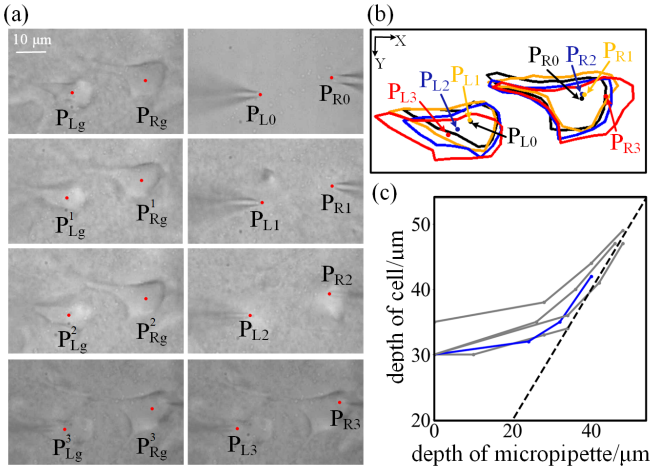

Fig. 6. Experimental process of dual-micropipette and dual-cell contact. (a) The sequential changes in the positions of the cells and micropipettes in microscopic images. (b) Extract and integrate the contours of cells and tips in (a). (c) The position relationship of the cells and micropipettes along the Z-axis.

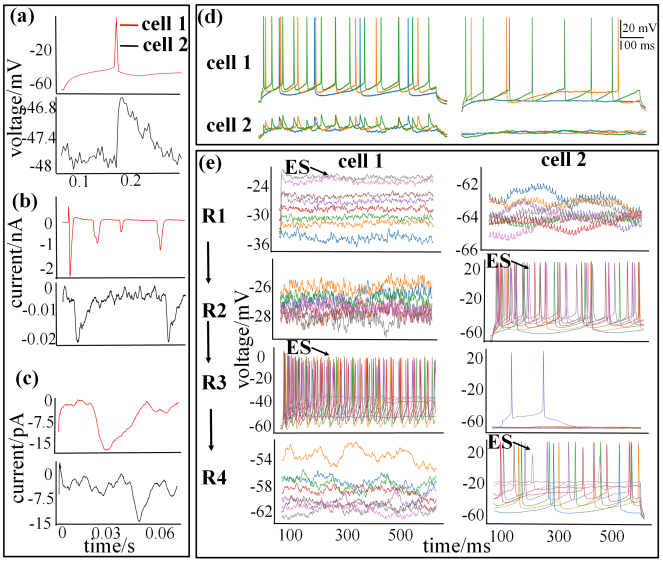

Fig. 7. Electrophysiological signals of double whole-cell recordings.

V. Discussion

In this paper, a robotic double patch clamp is proposed based on interactive mechanical modeling for functional connectivity measurement between neurons. However, due to artifacts in DIC imaging, the complexity of the brain environment, and interference from the micropipette, the three-dimensional localization of the cells is still performed manually. In future work, fully automated operation may be achieved by incorporating the 3D cell detecting and tracking algorithm [29].

The real cortical tissue exhibits heterogeneity and anisotropy at the microscopic level, partly due to layer-dependent variations in the vascular network. Large vessels are primarily located on the pial surface, while penetrating arterioles entering the cortex have micrometer-scale diameters and branch into capillaries with outer diameters peaking at 7–9 μm [30]. Since our experiments focused on a local region of the visual cortex and submillimeter scale deformation, the influence of vascular distribution on the model is limit. However, heterogeneity and anisotropy from other microstructures make the assumption of a homogeneous, isotropic viscoelastic medium an oversimplification, contributing to drift prediction errors and resulting in slight deviations when approaching the cells along the planned trajectory. Additionally, the model assumes micropipette motion quasi-statically, while viscoelastic tissues exhibit rate-dependent relaxation. Given that brain tissue relaxation time of 0.1–10 s [31] is shorter than the micropipettes approaching duration of 15 s, the tissue could sufficiently relax to near equilibrium, making the quasi-static approximation appropriate. Future work will incorporate anisotropic and rate-dependent viscoelastic models to better capture tissue mechanics and improve motion prediction accuracy.

In addition, the used methods still rely on traditional techniques including resistive contact detection based a fixed resistance threshold, constant-pressure gigaseal formation, and constant pulse-pressure break-in, which may suffer from poor excessive or insufficient contact, unstable sealing, and seal loosening during break-in in some cases. Therefore, in future work, both the resistance feedback and the membrane deformation of the cell should be detected during the contact stage to more accurately reflect the contact status and improve contact quality. During the sealing stage, the aspiration pressure could be dynamically adjusted based on real-time resistance feedback to achieve a tighter gigaseal. During the break-in stage, the effects of negative pressure pulse parameters on break-in efficiency and patch stability should be investigated to achieve low-disturbance break-in, ultimately improving the success rate of the double whole-cell recording.

This study is currently limited to brain slice environment, while in vivo experiments offer more complete neural connectivity and greater research significance. In in vivo experiments, cell staining, fluorescent micropipette labeling, and target detection techniques [11] are required to achieve automated localization of cells and micropipettes. Furthermore, given the increased complexity of interactive mechanical disturbances in vivo, the future work will also focus on improving the current mechanical interaction model.

At present, the low probability of functional connectivity between neurons limits the success rate of this method in detecting synaptic connections. In the future, pre-identifying synaptically connected neurons through staining techniques, followed by double recording using the approach proposed in this study, may significantly enhance the detection efficiency of functional connections.

VI. Conclusion

In this paper, an interactive mechanical modeling of two micropipette electrodes approaching two target cells in elastic environment was established to estimate the dynamic drift of two target cells. Based on the above model, an appropriate relative position of two target cells, a synchronous descent strategy of two micropipettes to two target cells and an online trajectory plan of two micropipettes were determined to reduce the dynamic drift of two cells for improving double patch clamp efficiency. Finally, a robotic double patch clamp operation process was established based on above work for functional connectivity measurement between neurons in brain slice. The effectiveness of the above work was validated through both FEM modeling and experimental results. The double patch clamp experiments on neurons in visual cortex demonstrate that our robotic double patch clamp system achieves a 40% improvement in success rate and a 38% improvement in operation speed in comparison to the traditional manual double patch clamp method. With the above advantages, diverse functional connectivity activities including action potential transmission and excitatory regulation between neurons in visual cortex were found using our system. The above finds prove the effectiveness of the proposed system which paves a solid ground for further functional connectivity research in alive brain.

References

[1] K. J. Friston, "Functional and effective connectivity: a review," *Brain connectivity*, vol. 1, no. 1, pp. 13–36, 2011.

[2] H. Eichenbaum, "Prefrontal–hippocampal interactions in episodic memory," *Nature Reviews Neuroscience*, vol. 18, no. 9, pp. 547–558, 2017.

[3] A. Chehade and K. Liu, "Structural degradation modeling framework for sparse data sets with an application on alzheimer's disease," *IEEE Transactions on Automation Science and Engineering*, vol. 16, no. 1, pp. 192–205, 2018.

[4] C. S. Bauer, R. N. Cohen, F. Sironi, M. R. Livesey, T. H. Gillingwater, J. R. Highley, D. J. Fillingham, I. Coldicott, E. F. Smith, Y. B. Gibson *et al.*, "An interaction between synapsin and c9orf72 regulates excitatory synapses and is impaired in als/ftd," *Acta Neuropathologica*, vol. 144, no. 3, pp. 437–464, 2022.

[5] E. Neher and B. Sakmann, "Single-channel currents recorded from membrane of denervated frog muscle fibres," *Nature*, vol. 260, no. 5554, pp. 799–802, 1976.

[6] R. Yang, Y. Fang, J. Yang, and K. W. C. Lai, "Design and analysis of electrical resistance feedback for automated patch clamp on adherent cells," *IEEE Transactions on Automation Science and Engineering*, vol. 14, no. 2, pp. 844–854, 2017.

[7] C. J. Milligan, J. Li, P. Sukumar, Y. Majeed, M. L. Dallas, A. English, P. Emery, K. E. Porter, A. M. Smith, I. McFadzean *et al.*, "Robotic multiwell planar patch-clamp for native and primary mammalian cells," *Nature protocols*, vol. 4, no. 2, pp. 244–255, 2009.

[8] S. B. Kodandaramaiah, G. T. Franzesi, B. Y. Chow, E. S. Boyden, and C. R. Forest, "Automated whole-cell patch-clamp electrophysiology of neurons in vivo," *Nature methods*, vol. 9, no. 6, pp. 585–587, 2012.

[9] S. Kodandaramaiah, F. Flores, G. Holst, A. Singer, X. Han, E. Brown, and C. Forest, "Multi-neuron intracellular recording in vivo via interacting autopatching robots. elife, 7," 2018.

[10] I. Kolb, W. Stoy, E. Rousseau, O. Moody, A. Jenkins, and C. Forest, "Cleaning patch-clamp pipettes for immediate reuse," *Scientific reports*, vol. 6, no. 1, p. 35001, 2016.

[11] L. A. Annecchino, A. R. Morris, C. S. Copeland, O. E. Agabi, P. Chadderton, and S. R. Schultz, "Robotic automation of in vivo two-photon targeted whole-cell patch-clamp electrophysiology," *Neuron*, vol. 95, no. 5, pp. 1048–1055, 2017.

[12] J.-S. Jouhanneau and J. F. Poulet, "Multiple two-photon targeted whole-cell patch-clamp recordings from monosynaptically connected neurons in vivo," *Frontiers in synaptic neuroscience*, vol. 11, p. 15, 2019.

[13] S. Yang and K. W. C. Lai, "Development of a dual arm microrobot for electrophysiological recording," in *2022 IEEE International Conference on Robotics and Biomimetics (ROBIO)*. IEEE, 2022, pp. 1485–1490.

[14] G. I. V. Gonzalez, P. O. Kgwarae, and S. R. Schultz, "Two-photon targeted, quad whole-cell patch-clamping robot," in *2023 11th International IEEE/EMBS Conference on Neural Engineering (NER)*. IEEE, 2023, pp. 1–5.

[15] J. Hao and P. Delmas, "Recording of mechanosensitive currents using piezoelectrically driven mechanostimulator," *Nature protocols*, vol. 6, no. 7, pp. 979–990, 2011.

[16] A. H. Lewis and J. Grandl, "Stretch and poke stimulation for characterizing mechanically activated ion channels," *Methods in Enzymology*, vol. 654, pp. 225–253, 2021.

[17] B. Ma, C. Cui, R. Li, M. Li, J. Qiu, K. Li, M. Sun, X. Zhao, and Q. Zhao, "Robotic dual-arm patch clamp for neuron excitability research under mechanical stimulation," in *2024 43rd Chinese Control Conference (CCC)*. IEEE, 2024, pp. 7522–7527.

[18] B. Ma, J. Qiu, C. Cui, K. Li, R. Li, M. Li, Y. Liu, S. Fu, M. Sun, X. Zhao *et al.*, "Robotic fast dual-arm patch clamp system for mechanosensitive excitability research of neurons," *IEEE transactions on bio-medical engineering*, vol. 72, no. 2, pp. 822–832, 2025.

[19] J. Wang, X. Li, J. Zheng, and D. Sun, "Dynamic path planning for inserting a steerable needle into a soft tissue," *IEEE/ASME Transactions on Mechatronics*, vol. 19, no. 2, pp. 549–558, 2013.

[20] Q. Zhao, J. Qiu, Z. Feng, Y. Du, Y. Liu, Z. Zhao, M. Sun, M. Cui, and X. Zhao, "Robotic label-free precise oocyte enucleation for improving developmental competence of cloned embryos," *IEEE Transactions on Biomedical Engineering*, vol. 68, no. 8, pp. 2348–2359, 2020.

[21] R. Li, M. Li, J. Qiu, K. Li, Y. Liu, C. Cui, S. Fu, B. Ma, Q. Zhang, M. Cui *et al.*, "Precise robotic picking up of polar body for biopsy application," *IEEE Transactions on Automation Science and Engineering*, 2024.

[22] Q. Zhao, J. Qiu, Y. Han, Y. Jia, Y. Du, H. Gong, M. Li, R. Li, M. Sun, and X. Zhao, "Robotic patch clamp based on noninvasive 3-d cell morphology measurement for higher success rate," *IEEE Transactions on Instrumentation and Measurement*, vol. 71, pp. 1–12, 2022.

[23] K. Miller and K. Chinzei, "Mechanical properties of brain tissue in tension," *Journal of biomechanics*, vol. 35, no. 4, pp. 483–490, 2002.

[24] J. Qiu, Q. Zhao, R. Li, Y. Liu, B. Ma, and X. Zhao, "Robotic fast patch clamp in brain slices based on stepwise micropipette navigation and gigaseal formation control," *Sensors*, vol. 25, no. 4, p. 1128, 2025.

[25] J. Shi, D. Zuo, and Z. Zhang, "Transition activity recognition system based on standard deviation trend analysis," *Sensors*, vol. 20, no. 11, p. 3117, 2020.

[26] C.-Y. Wang, A. Bochkovskiy, and H.-Y. M. Liao, "Yolov7: Trainable bag-of-freebies sets new state-of-the-art for real-time object detectors," in *Proceedings of the IEEE/CVF conference on computer vision and pattern recognition*, 2023, pp. 7464–7475.

[27] L. Campagnola, S. C. Seeman, T. Chartrand, L. Kim, A. Hoggarth, C. Gamlin, S. Ito, J. Trinh, P. Davoudian, C. Radaelli *et al.*, "Local connectivity and synaptic dynamics in mouse and human neocortex," *Science*, vol. 375, no. 6585, p. eabj5861, 2022.

[28] J. Stedehouder, B. M. Roberts, S. Raina, S. Bossi, A. K. L. Liu, N. M. Doig, K. McGerty, P. J. Magill, L. Parkkinen, and S. J. Cragg, "Rapid modulation of striatal cholinergic interneurons and dopamine release by satellite astrocytes," *Nature Communications*, vol. 15, no. 1, p. 10017, 2024.

[29] H. Gong, J. Qiu, L. Li, Y. Yao, Q. Zhao, X. Zhao, and M. Sun, "Positioning and tracking of neurons in label-free tissue slice for automatic patch clamping," in *2021 IEEE International Conference on Robotics and Biomimetics (ROBIO)*. IEEE, 2021, pp. 49–54.

[30] R. Saiga, M. Uesugi, A. Takeuchi, K. Uesugi, Y. Suzuki, S. Takekoshi, C. Inomoto, N. Nakamura, Y. Torii, I. Kushima *et al.*, "Brain capillary structures of schizophrenia cases and controls show a correlation with their neuron structures," *Scientific Reports*, vol. 11, no. 1, p. 11768, 2021.

[31] B. Babaei, A. Davarian, K. M. Pryse, E. L. Elson, and G. M. Genin, "Efficient and optimized identification of generalized maxwell viscoelastic relaxation spectra," *Journal of the mechanical behavior of biomedical materials*, vol. 55, pp. 32–41, 2016.

Biting Ma Biting Ma received a bachelor's degree in Intelligent Medical Engineering from Nankai University. She is currently pursuing her Ph.D. degree with the College of Artificial Intelligence, Nankai University, Tianjin, China. Her research interests include robotic dual-arm patch clamp systems, micromanipulators and microsystems.

Jinyu Qiu Jinyu Qiu received the Ph.D. degree in control science and technology from Nankai University, Tianjin, China, in 2025. He was also a visiting student at Imperial College London from 2022 to 2023. He is currently a post-doctoral researcher with the College of Artificial Intelligence, Nankai University. His research interests include robotic patch clamp system, micromanipulators and microsystems.

Yiwen Liu Yiwen Liu received the B.S. degree in computer science and technology from the Nankai University, Tianjin, China, in 2022. He is currently working toward the Ph.D. degree in artificial intelligence with Nankai University, Tianjin, China. His current research interests include computer vision and underwater image segmentation.

Ruimin Li Ruimin Li received the B.Eng. degree in Intelligence Science and Technology, Hebei University of Technology, Tianjin, China, in 2022. She is currently pursuing her Ph.D. degree in control science and engineering with Nankai University, Tianjin, China. Her research interests include robotic patch clamp systems, micromanipulators and microsystems.

Shaojie Fu Shaojie Fu is received the B.Eng.degree in automation from Taiyuan University of Technology, Taiyuan. China, in 2023. He is currently pursuing his Ph.D. degree with the College of Artificial Intelligence, Nankai University. His research interests are micromanipulators and microsystems.

Yuzhu Liu Yuzhu Liu received the bachelor's degree in NUAA's College of Automation Engineering, Nanjing, China, in 2022. She is currently pursuing her doctor's degree in artificial intelligence with Nankai University, Tianjin, China. Her research interests include robotic patch clamp system and micromanipulators.

Hao Chen Hao Chen received his B.S. degree from Jiangnan University in 2022 and his M.S. degree from Qilu University of Technology (Shandong Academy of Sciences) in 2024. He is currently pursuing a Ph.D. at the School of Artificial Intelligence, Nankai University. His research interests include flexible strain sensors and microelectrode arrays in brain science.

Mingzhu Sun Mingzhu Sun (Member, IEEE) received the B.S. degree in computer science and technology, the M.S. degree in computer application, and the Ph.D. degree in control theory and control engineering from Nankai University, Tianjin, China, in 2003, 2006, and 2009, respectively. She joined the Faculty of Nankai University in 2009. She is currently a Professor and the Deputy Director of the Institute of Robotics and Automatic Information System. Her research interests include micromanipulation, image processing, and computer vision.

Xin Zhao Xin Zhao (Member, IEEE) received the B.S. degree in control theory and control engineering from Nankai University, Tianjin, China, in 1991, the M.S. degree in control theory and control engineering from Shenyang Institute of Automation, CAS, Shenyang, China, in 1994, and the Ph.D. degree in control theory and control engineering from Nankai University in 1997. In 1997, he joined Nankai University, where he is currently a Professor and the Dean of the College of Artificial Intelligence. His research interests include micromanipulation, microsystems, and mathematical biology.

Qili Zhao Qili Zhao (Member, IEEE) received the Ph.D. degree in control theory and control engineering from Nankai University, Tianjin, China, in 2014. He was a Post-Doctoral Researcher with the Robotics and Mechatronics Research Laboratory, Department of Mechanical and Aerospace Engineering, Monash University, Melbourne, VIC, Australia, from 2014 to 2015, and a Post-Doctoral Fellow with the Advanced Micro and Nanosystems Laboratory, Department of Mechanical and Industrial Engineering, University of Toronto, Toronto, ON, Canada, from 2015 to 2018. He is currently an Associate Professor with the College of Artificial Intelligence, Nankai University. His current research interests include robotic patch clamp, robotic cell manipulation, and robotic cell measurement.